(2)

CONFINEMENT

---Quarks, the fundamental particle, cannot live in the "physical vacuum", which is a complex many-body state containing large amplitudes of gluon fields, etc.
---Quarks build a bag of "real" vacuum inside the nucleon.

---Inside the CuO_2 planes is the "physical vacuum", a complex many-body state in which electrons are not elementary excitations. Rather, electrons are unstable, breaking up into spinons and holons.
---Only electrons can live in the real vacuum, which inhabits ordinary metals and the intervening insulating layers.
---In-plane charge transport is by holon motion.
---Transport between planes is only by electrons, which requires the holon and spinon to reassemble into an electron before interlayer transport.

THE Theory of SUPERCONDUCTIVITY in the High-Tc Cuprates,
P.W. Anderson (Princeton Univ. Press, 1997) ISBN 0-691-04365-5

Boebinger
Lecture 2

(1)

ABNORMAL NORMAL STATE of the HIGH-Tc's
(and WHY USE HIGH MAGNETIC FIELDS ?)

LOW - DIMENSIONAL TRANSPORT
and QUASI-PARTICLE CONFINEMENT

REVEALING QUANTUM CRITICAL POINTS
in the HIGH-Tc PHASE DIAGRAM

SCIENCE, Correlated Electron Systems, 21 April 2000
"Advances in the Physics of High-Temperature Superconductivity"
J. Orenstein and A.J. Millis, Science 288 (2000) 468
"Quantum Criticality: Competing Ground States in Low Dimensions"
Subir Sachdev, Science 288 (2000) 475
"Sources of Quantum Protection in High-Tc Superconductivity"
Philip W. Anderson, Science 288 (2000) 480

THE Theory of SUPERCONDUCTIVITY in the High-Tc Cuprates,
P.W. Anderson (Princeton Univ. Press, 1997) ISBN 0-691-04365-5

(3)

Evidence of CONFINEMENT in ARPES data

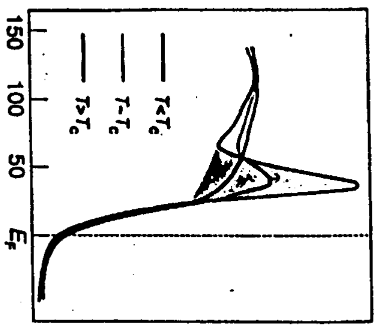

Fig. 4. Representation of ARPES spectra [adapted from (72, 73)] for underdoped high-T_c superconductor at momentum near the (0,π) or "antinodal" point of the Brillouin zone. Shown is photoemission intensity (proportional to the probability of finding an electron at the given momentum and energy) at fixed momentum, as a function of energy measured relative to E_F.

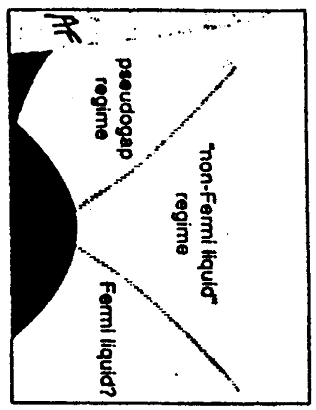

In the overdoped regime, the quasiparticle peak broadens slightly above Tc, due to increased phase space for scattering when the superconducting gap collapses.
In the underdoped regime, the quasiparticle peak disappears at Tc, and the energy gap persists above Tc *as if the quasiparticle owes its existence to the phase coherence of the superconducting state.*

A.G. Loeser, et al, PRB 56 (1997) 14185
A.V. Fedorov, et al. PRL 82 (1999) 217

CONTRASTING ρ_{ab} AND ρ_c IN Bi-2201

RAPID COMMUNICATIONS
PHYSICAL REVIEW B VOLUME 41, NUMBER 1 1 JANUARY 1990

Normal-state transport properties of $Bi_{2+x}Sr_{2-y}CuO_{6\pm\delta}$ crystals

S. Martin, A. T. Fiory, R. M. Fleming, L. F. Schneemeyer, and J. V. Waszczak
AT&T Bell Laboratories, Murray Hill, New Jersey 07974

(Received 19 September 1989)

Transport anisotropies of $\rho_c/\rho_{ab}\approx 10^4$ to 10^5 were measured for superconducting and nonsuperconducting $Bi_{2+x}Sr_{2-y}CuO_{6\pm\delta}$ crystals. In superconducting samples ρ_{ab} increases linearly with temperature from just above $T_c\approx 7$ to 700 K. The implication of the ρ_{ab} results is that classical electron-phonon scattering mechanisms are inadequate. The anisotropy and T_c for various layered superconductor systems are compared. In all crystals studied ρ_c is nonmetallic, varying as a power law $T^{-\alpha}$, $\alpha\approx 0.5-1$.

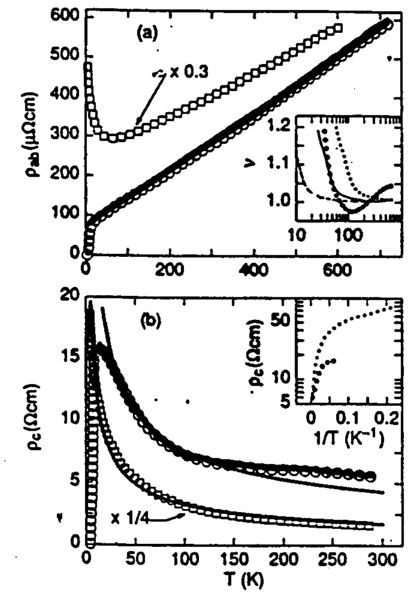

FIG. 1. In-plane (a) and out-of-plane (b) resistivities measured in 2:2:0:1 crystals: a nonsuperconductor (□) grown with Sr/Bi = 1.22 and P_{O_2} = 20%, and a superconductor (○), with Sr/Bi = 1.0 and P_{O_2} = 4%. Curve in (a) is a fit assuming BG; curves in (b) are power-law fits. Inset (a) shows $\nu = d[\ln(\rho_{ab}-\rho_0)]/d[\ln T]$ vs T for the superconducting sample (●) as compared with BG fits with $\Theta_D^* = 10$ K (dashed), 35 K (solid), and 80 K (dotted). Inset (b) illustrates ρ_c is non-Arrhenius.

(5) 3

$La_{2-x}Sr_xCuO_4$

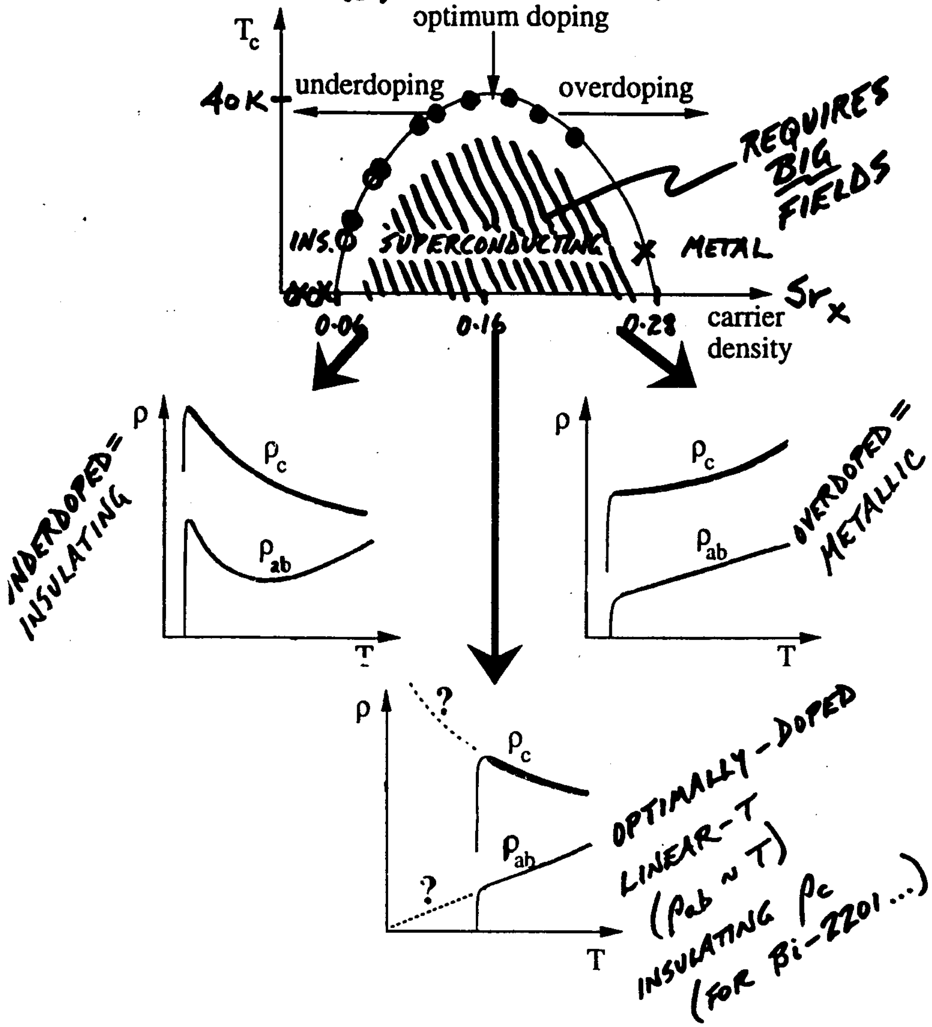

(6)

lsco_sum/xx-fig1d.org

INSULATOR–TO–METAL CROSSOVER IN THE NORMAL STATE OF A HIGH-Tc SUPERCONDUCTOR

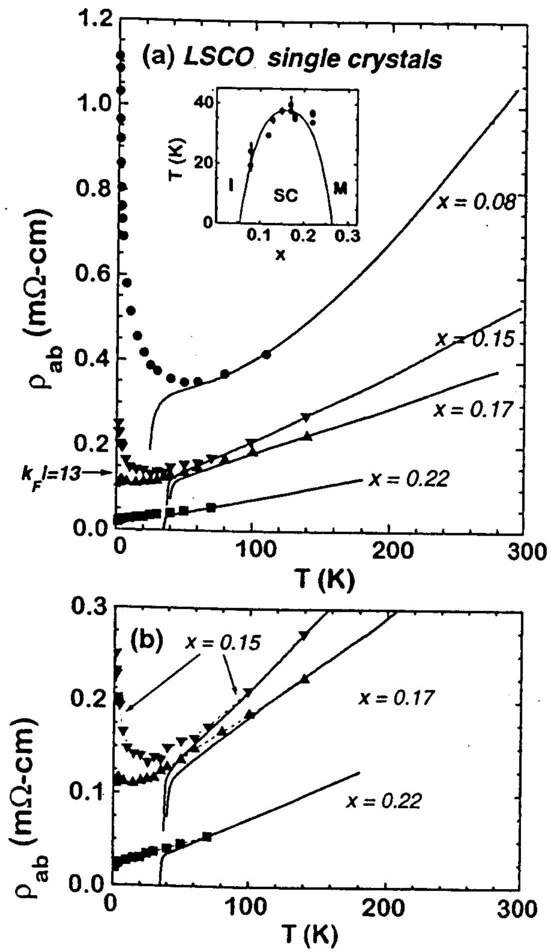

Boebinger, et al. PRL 77, 5417 (1996)

(7)

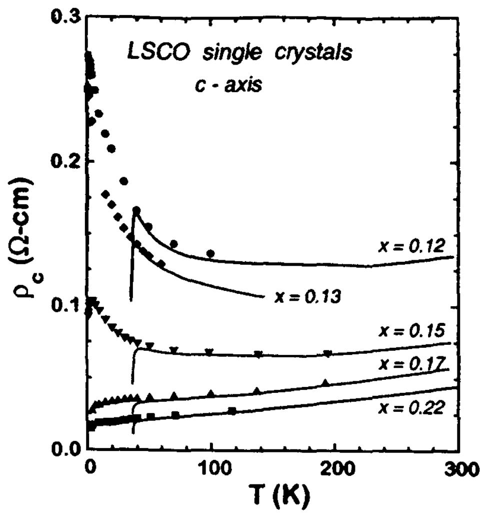

(8)

$La_{2-x}Sr_xCuO_4$

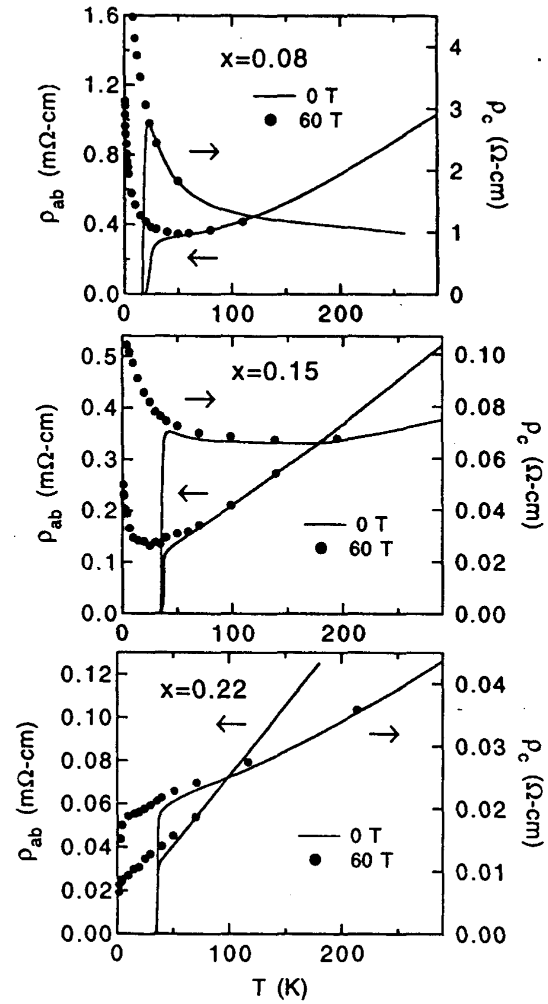

(9)

i:/lsco_sum/xmifig3b.org

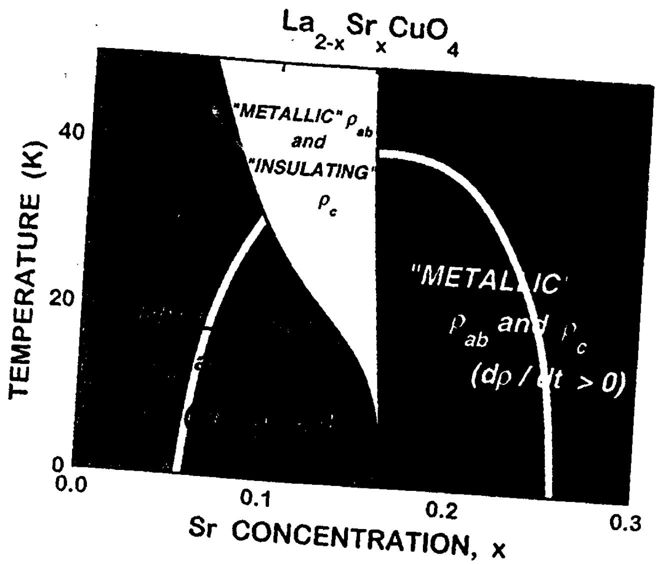

(10.)

$La_{2-x}Sr_xCuO_4$ $\frac{\rho_c}{\rho_{ab}} \sim 10^3$

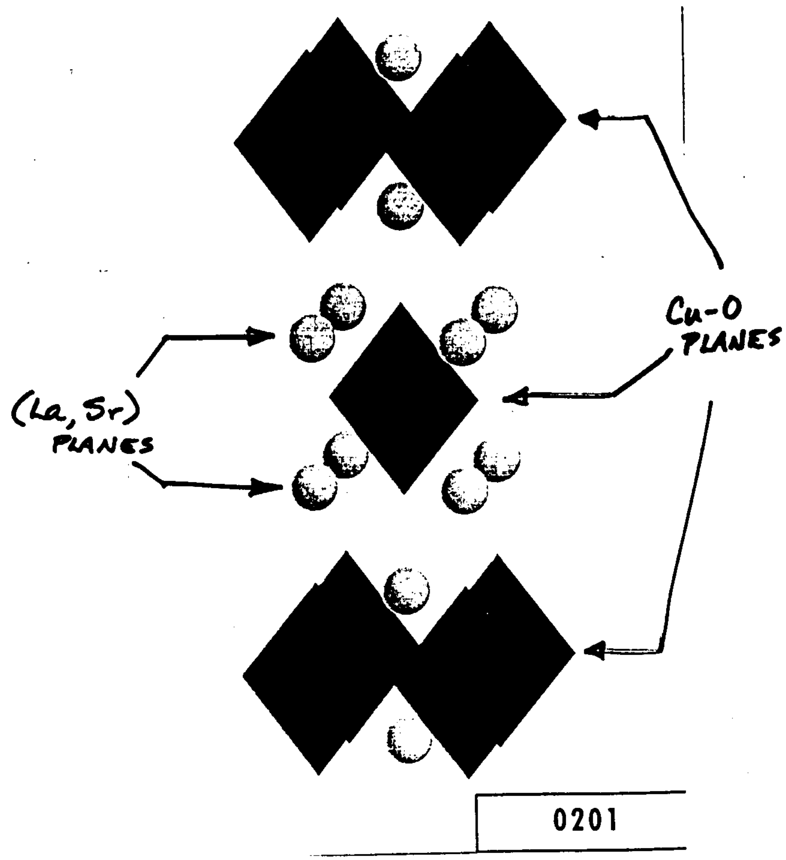

(11)

$Bi_2Sr_2CuO_y$ $\frac{\rho_c}{\rho_{ab}} \sim 10^4$

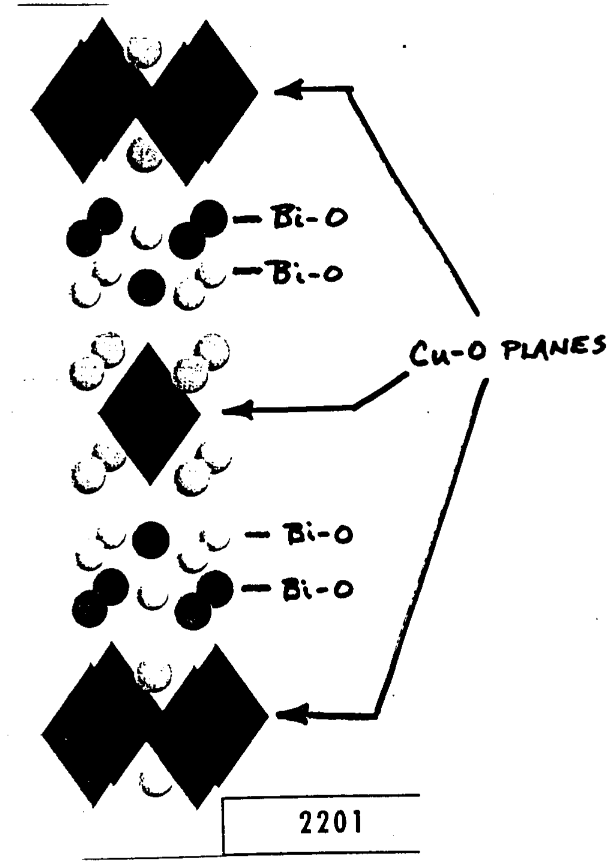

NEARLY 2D FERMI SURFACE

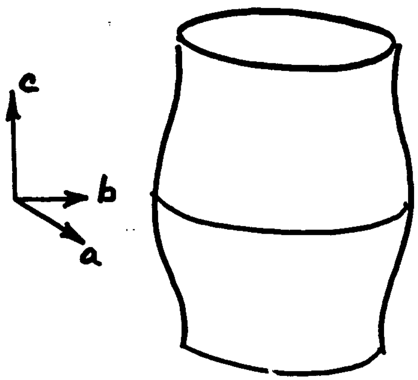

$$t_c \sim t_{ab}\left[\frac{\rho_{ab}}{\rho_c}\right]^{1/2}$$

10,000K

10^{-4}

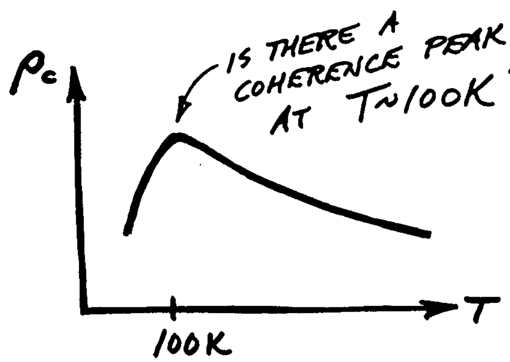

Sr_2RuO_4 ($T_c \sim 1$ K) ISOSTRUCTURAL WITH LSCO

INSULATING ρ_c
METALLIC ρ_{ab} } → 3D METAL AT LOW T

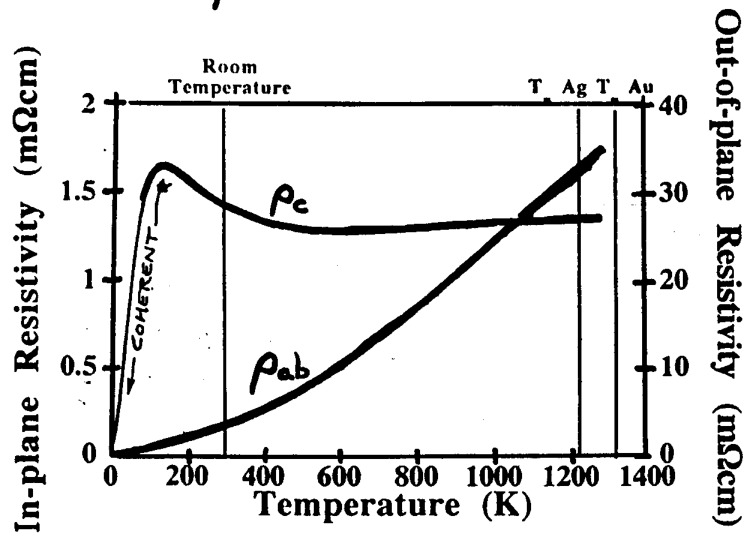

TYLER, MACKENZIE – CAMBRIDGE
NISHIZAKI – KYOTO
FUJITA, MAENO – HIROSHIMA

MEASUREMENT GEOMETRIES

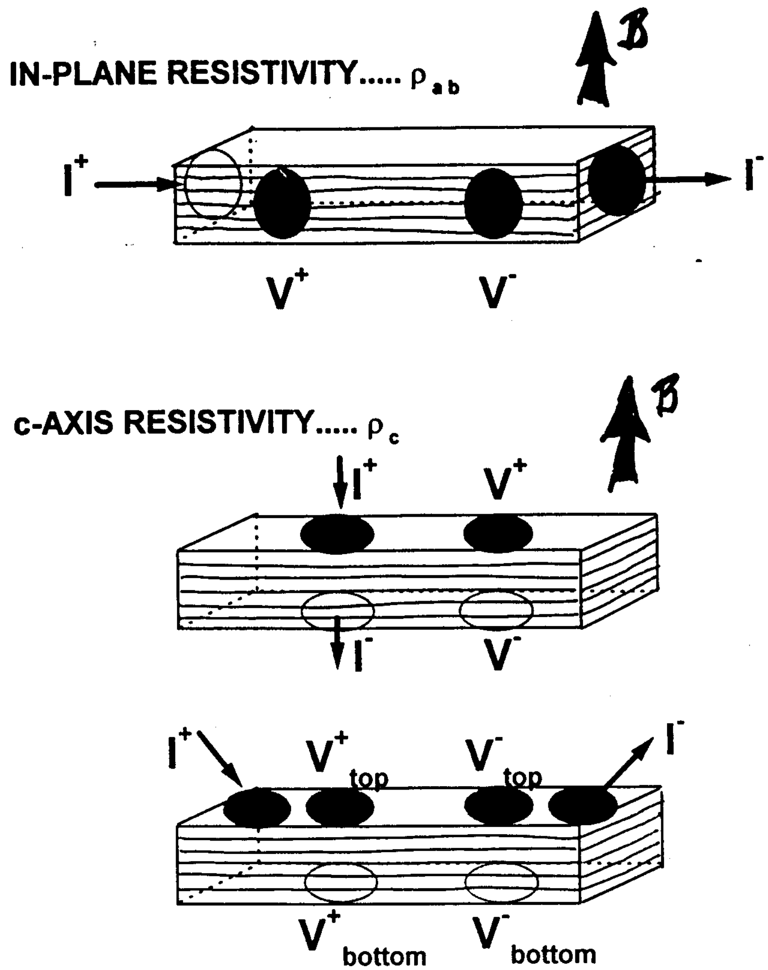

No Heating Effect at 0.7 K

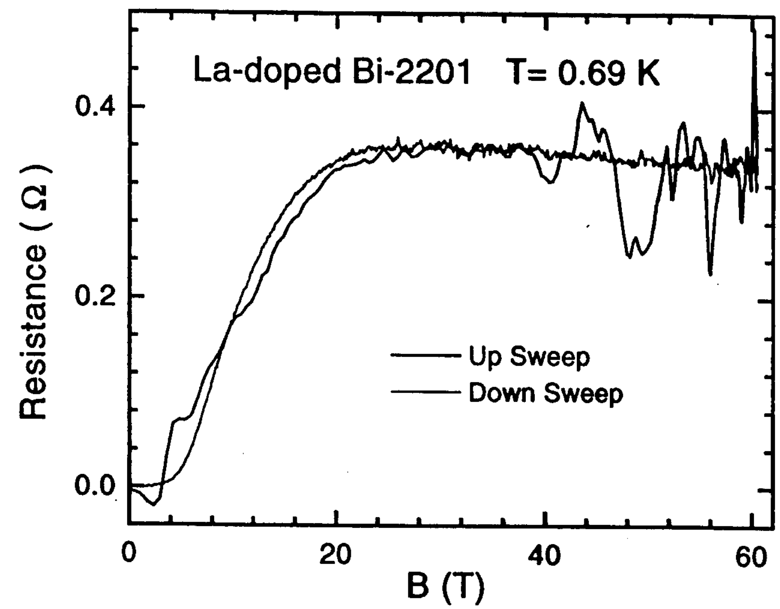

Eddy-current heating is proportional to $(dB/dt)^2$ and therefore is very different between up and down sweeps

(16)

La: Bi-2201

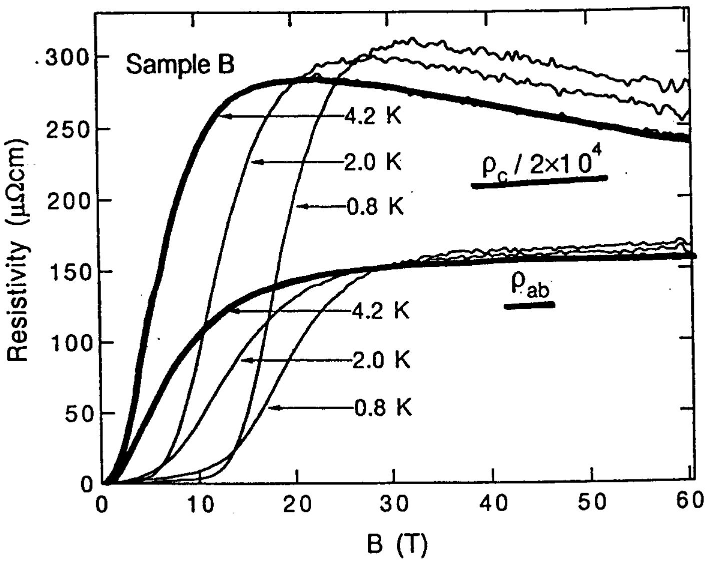

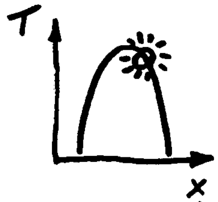

(17)

SAMPLE VARIATIONS in Bi-2201

La:Bi-2201(slightly overdoped)

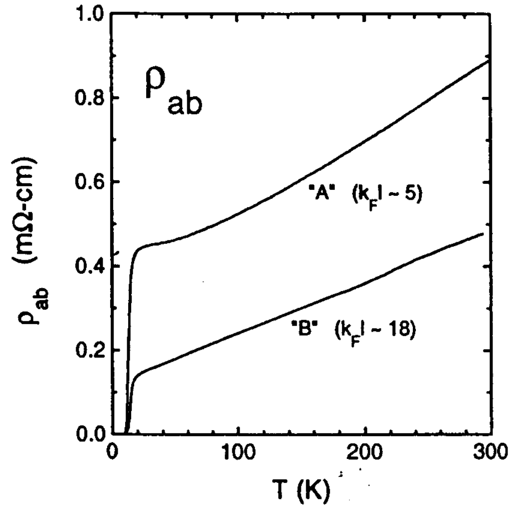

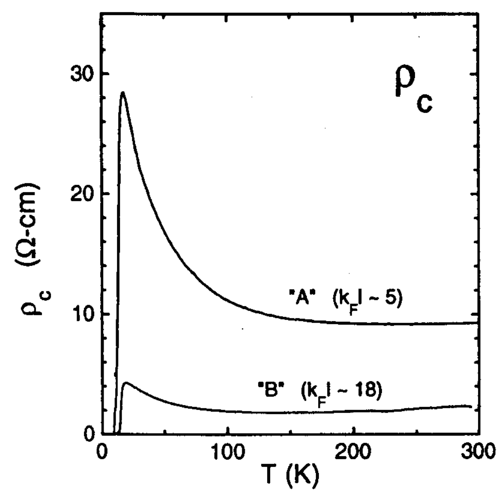

(18)

SAMPLE VARIATIONS in Bi-2201

La:Bi-2201(slightly overdoped)

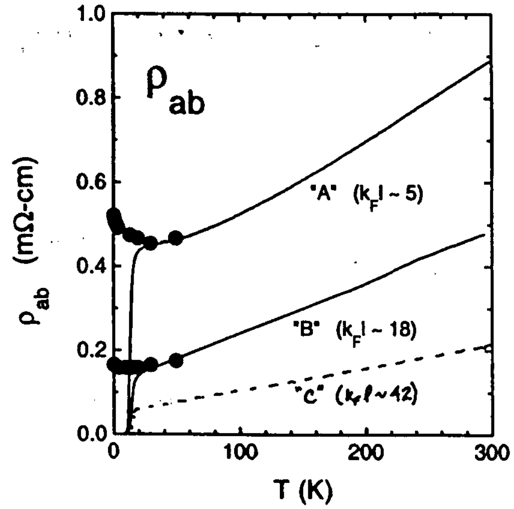

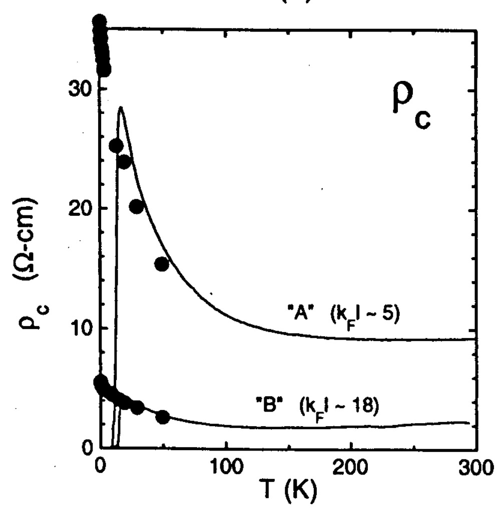

sample 2-5 (19)

LOGARITHMIC DIVERGENCE in Bi-2201

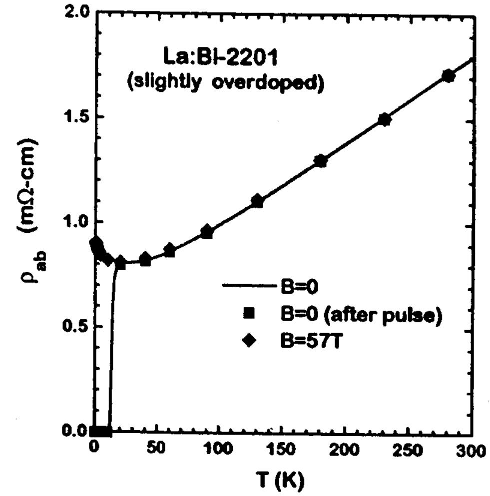

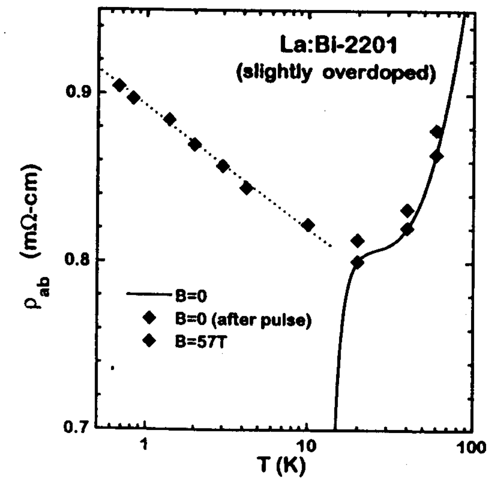

CUT TITLE

(20)

Is the normal state in Bi-2201 a Fermi Liquid?

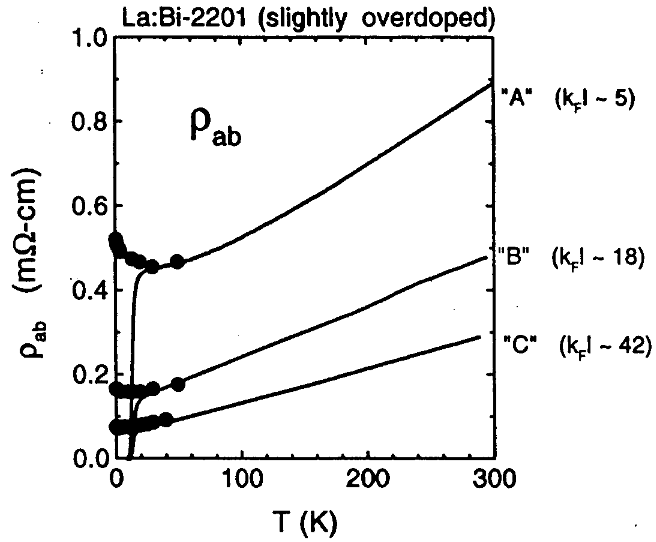

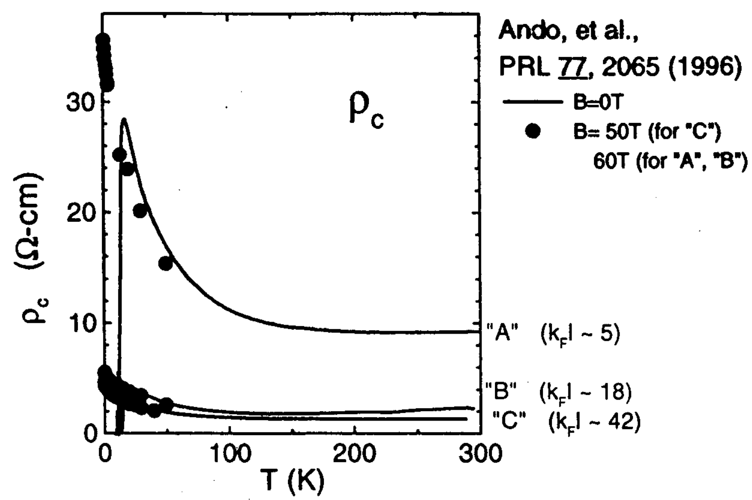

(21) AND 5

Metallic ρ_{ab} and diverging ρ_c can coexist at low temperatures in Bi-2201

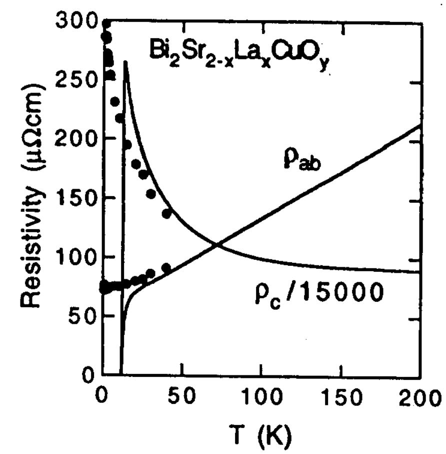

ANDO, et al
PRL 77 2065
(1996)

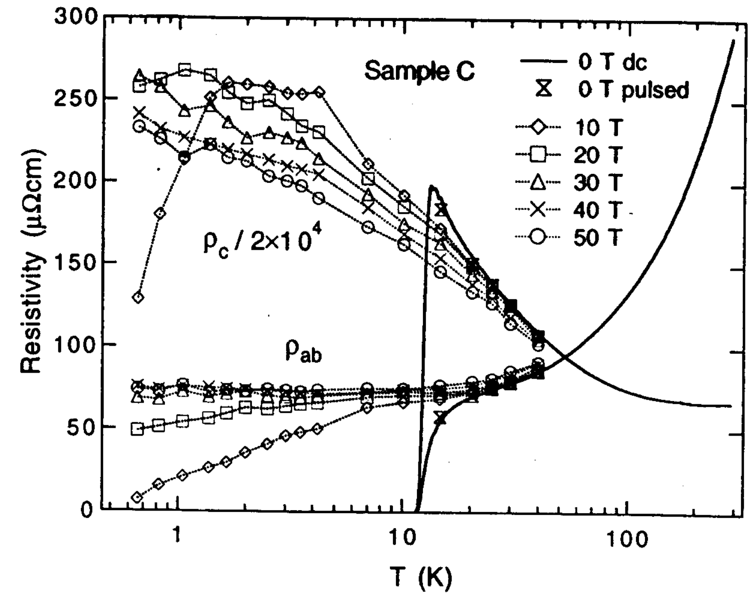

Implications of sample C

In conventional systems, ρ_{ab} and ρ_c behave the same way at low temperatures.

Fermi-liquid models for "semiconducting" ρ_c are likely to have difficulties with the data.

For Example,

- Phonon-assisted hopping model
  [Rojo and Levin, PR B 48, 16861 (1993)]

⇒ ρ_c must cross over to metallic behavior as phonon disappear at low temperatures, roughly T < 20 K.

Non-Fermi-liquid models seem consistent with the data.

- Resonanting Valence Bond theory
  [N. Nagaosa, PR B 52, 10561 (1995)]
- Luttinger Liquid theory
  [D.G. Clarke, S.P. Strong, and P.W. Anderson, PRL 74, 4499 (1995)]

In-plane quasiparticle confinement
(e.g. spinon-holon separation)
⇒ Incoherent c-axis transport, Coherent in-plane transport

CONCLUSIONS IN 1 FIGURE

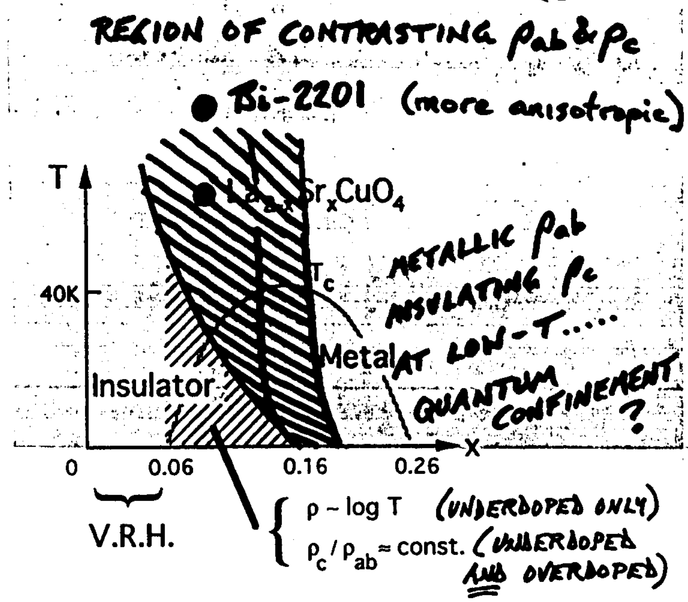

"CONCLUSIONS"

$(La,Sr)_2CuO_4$ and $YBa_2Cu_3O_{7-\delta}$

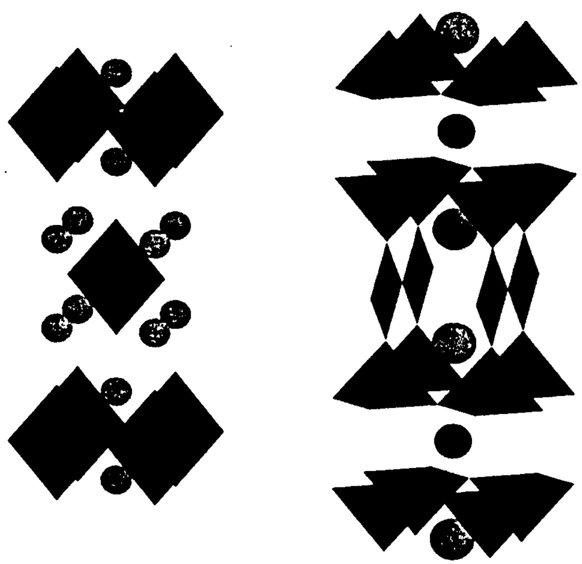

50K YBCO from Y. Ando

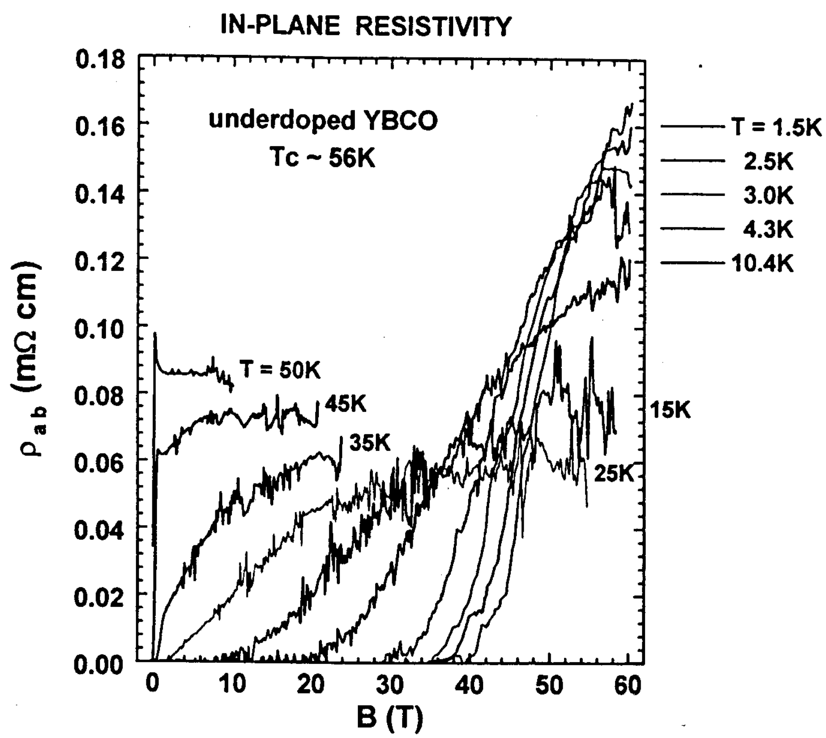

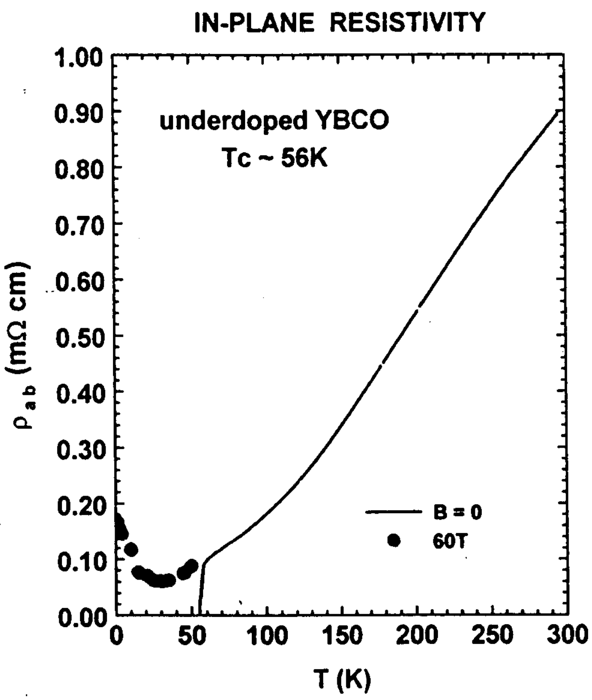
IN-PLANE RESISTIVITY
underdoped YBCO
Tc ~ 56K
B = 0
60T
ρ_{ab} (mΩ cm)
T (K)
1.00
0.90
0.80
0.70
0.60
0.50
0.40
0.30
0.20
0.10
0.00
0
50
100
150
200
250
300

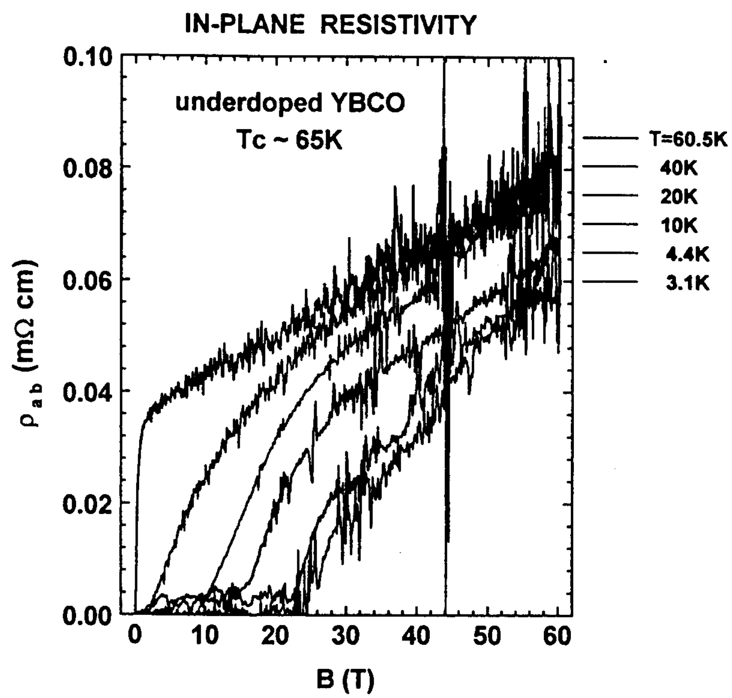
IN-PLANE RESISTIVITY
underdoped YBCO
Tc ~ 65K
T=60.5K
40K
20K
10K
4.4K
3.1K
ρ_{ab} (mΩ cm)
B (T)
0.10
0.08
0.06
0.04
0.02
0.00
0
10
20
30
40
50
60

28

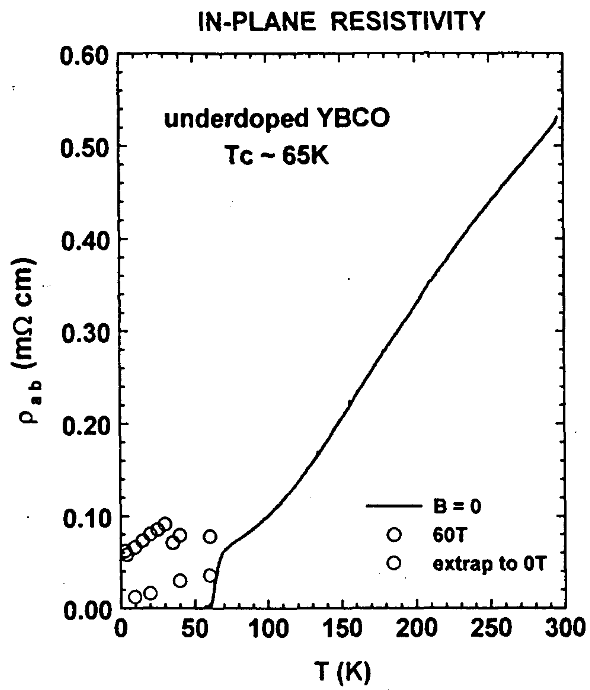

IN-PLANE RESISTIVITY
underdoped YBCO
Tc ~ 65K
ρ ab (mΩ cm)
0.60
0.50
0.40
0.30
0.20
0.10
0.00
0
50
100
150
200
250
300
T (K)
B = 0
60T
extrap to 0T

29

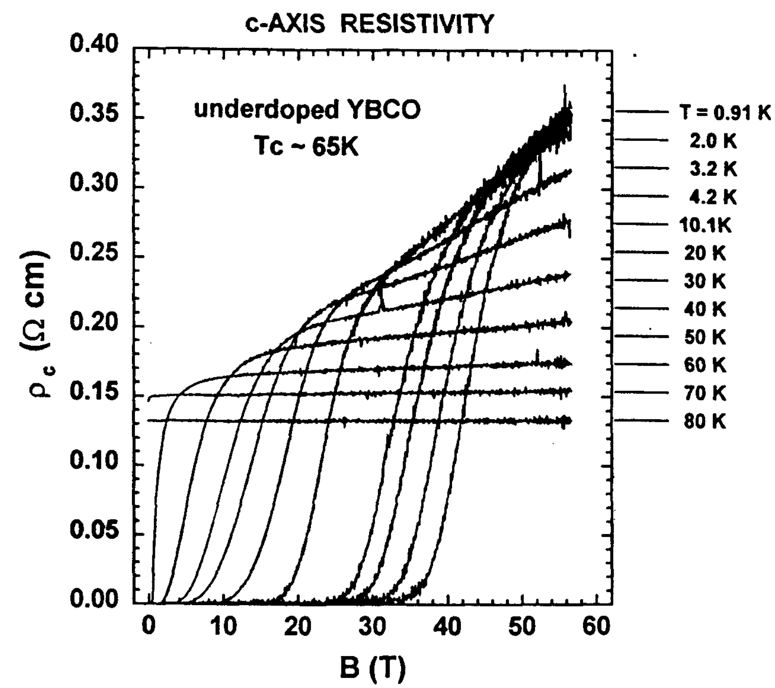

c-AXIS RESISTIVITY
underdoped YBCO
Tc ~ 65K
ρ c (Ω cm)
0.40
0.35
0.30
0.25
0.20
0.15
0.10
0.05
0.00
0
10
20
30
40
50
60
B (T)
T = 0.91 K
2.0 K
3.2 K
4.2 K
10.1K
20 K
30 K
40 K
50 K
60 K
70 K
80 K

underdoped YBCO Tc ~ 65K

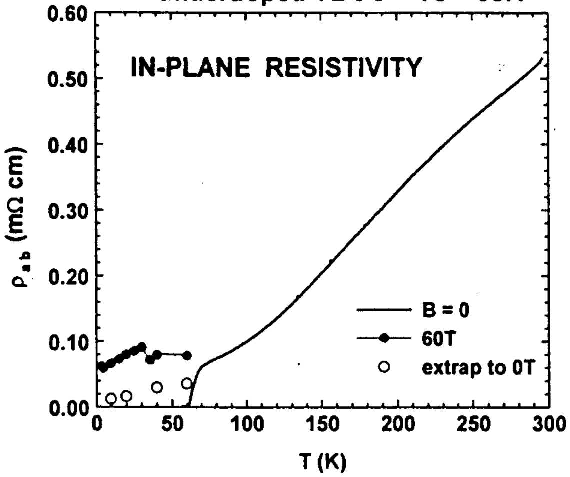

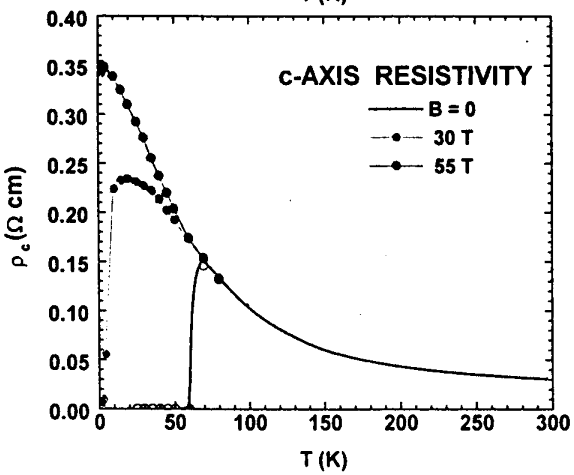

NORMAL STATE PHASE DIAGRAMS

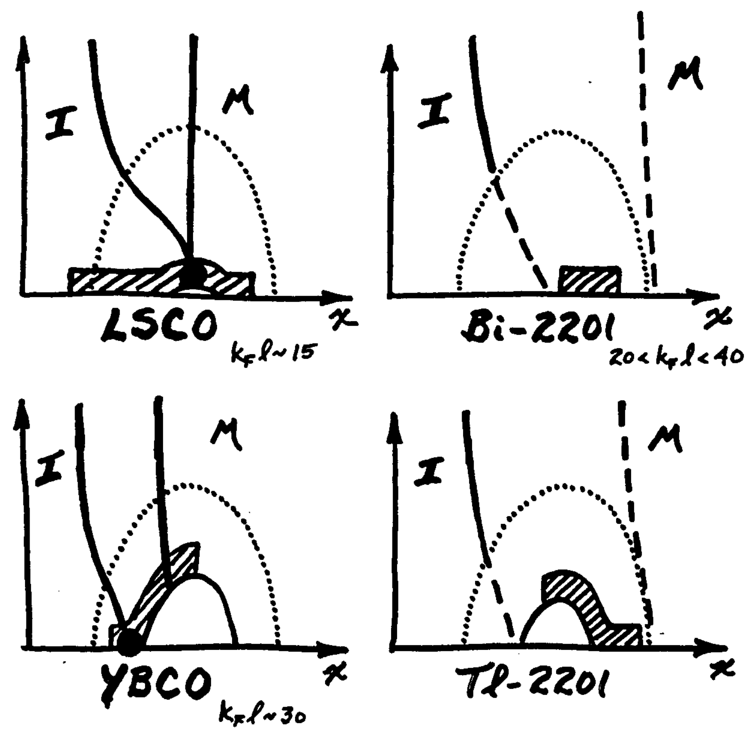

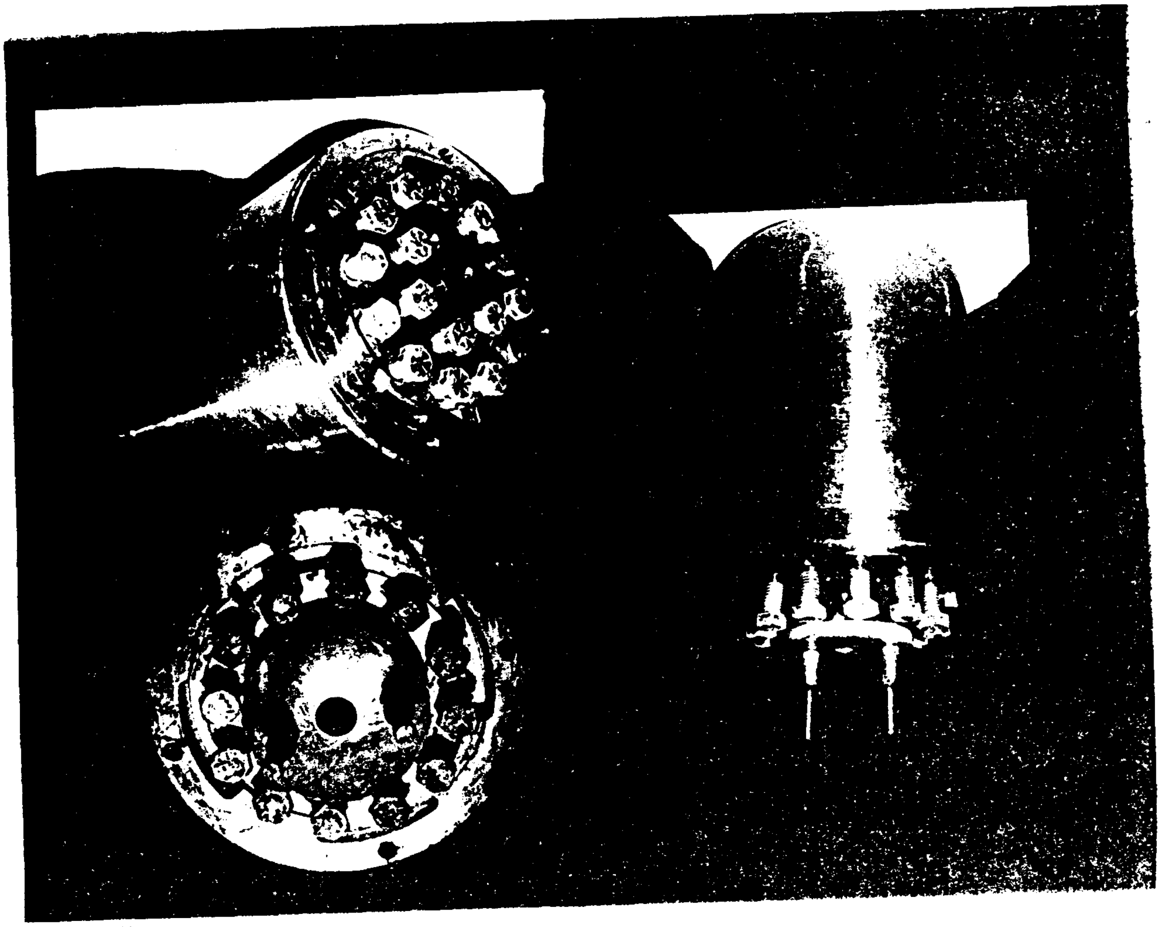

32

TOP
DO NOT AFFIX OVERLAYS ALONG THIS SURFACE

VG. NO.

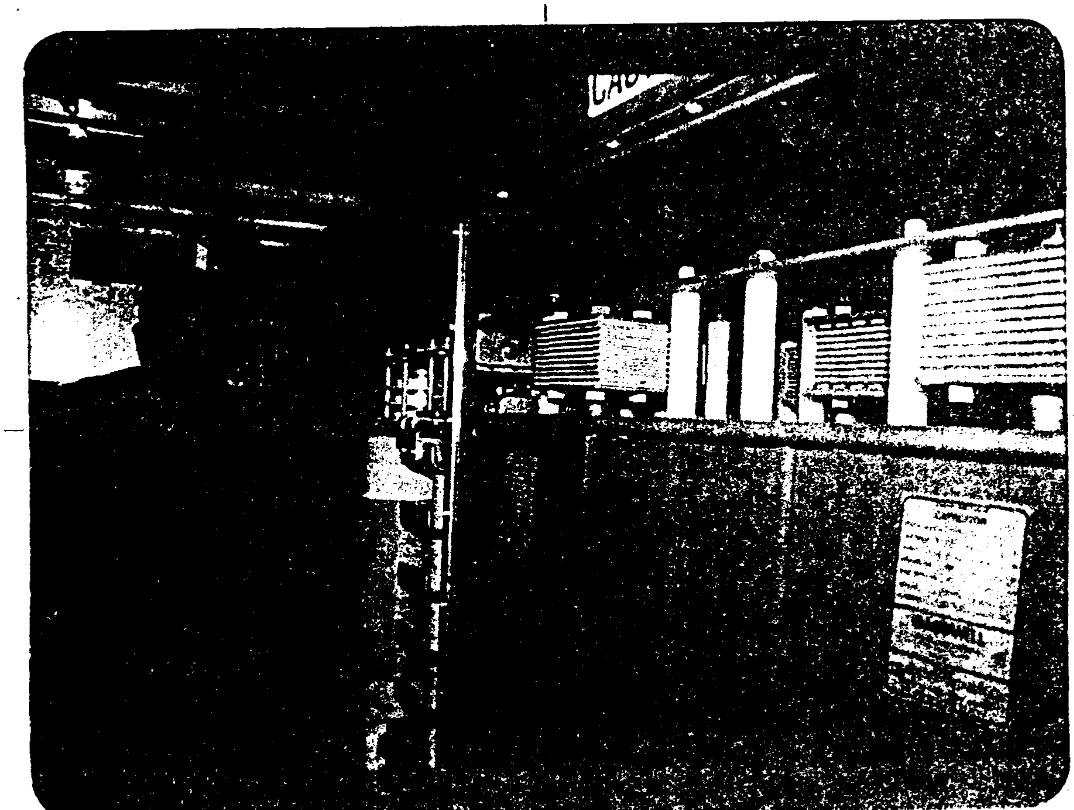

33

E-9148 (6 85)

34

National High Magnetic Field Laboratory
Pulsed Magnetic Field Facility

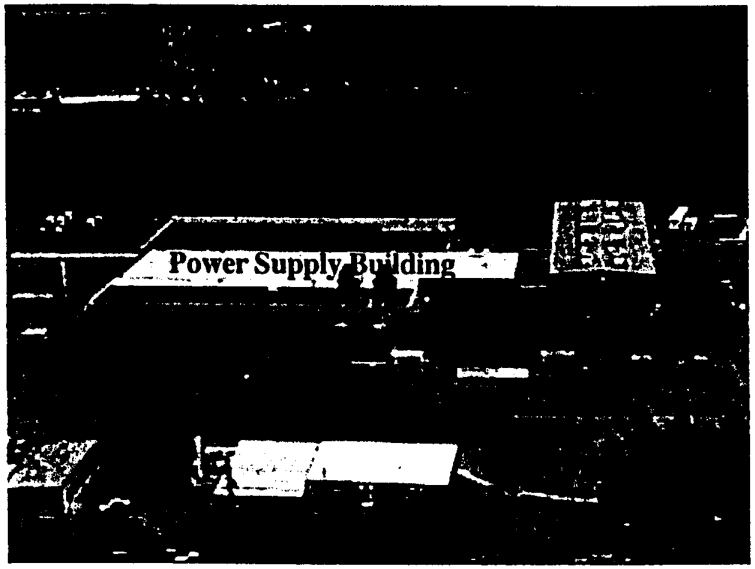

35

NHMFL Pulsed Magnet Facility in Los Alamos

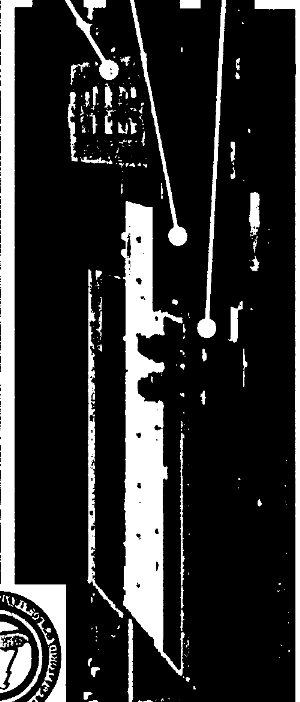

Generator Building

Long-Pulse Magnet Building

New Experimental Hall

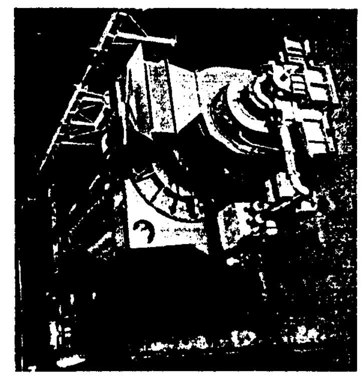

1.4 GVA Generator

(37)

NHMFL Pulsed Magnet Facility in Los Alamos

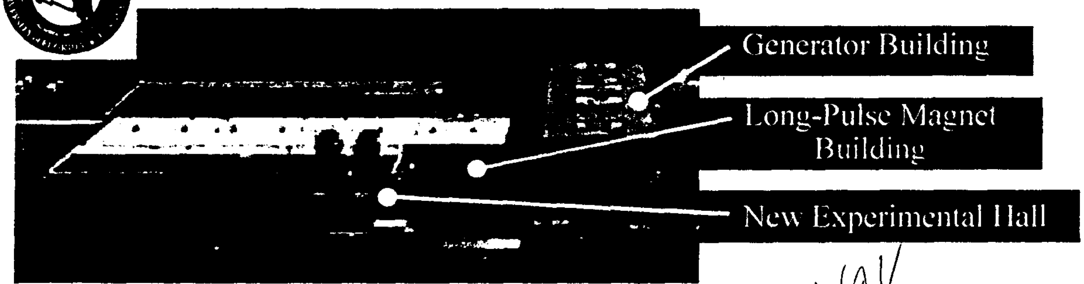

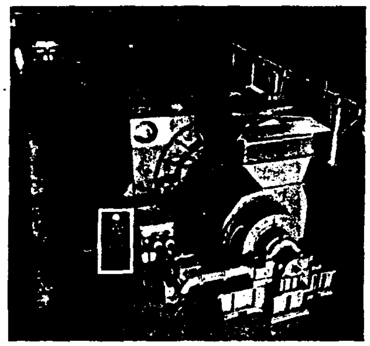

1.4 GVA Generator
(man in foreground)

Evacuate Long-Pulse Magnet Building
Spin up to 1650 rpm the 200,000 kg Rotor of the 1.4 GVA Generator
Click the Mouse on the Control Computer
Wait one second while the Generator spins down to ~1400rpm in one second..... and 250MJ is shoveled into the Long-Pulse Magnet Building

(36)

NHMFL 60T Long-Pulse Magnet in Los Alamos

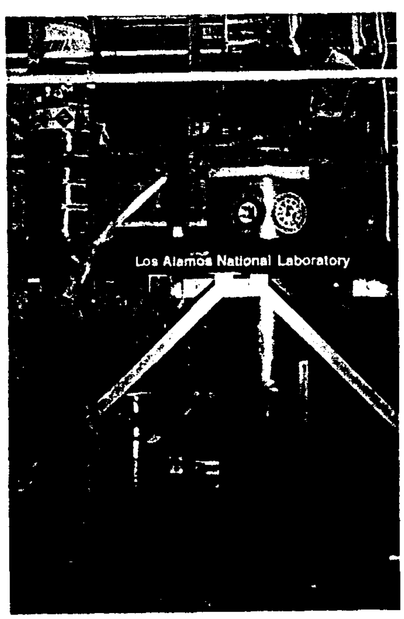

(39)

NHMFL Pulsed Magnet Facility in Los Alamos

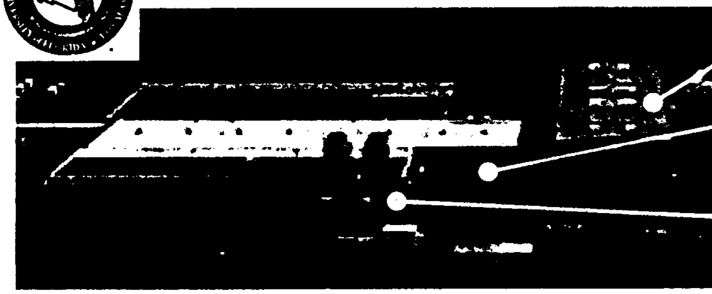

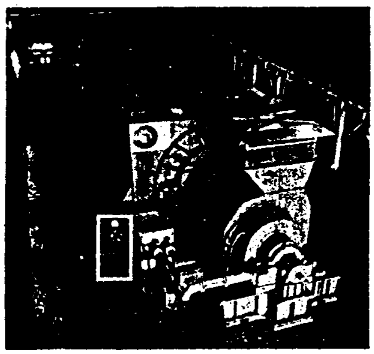

1.4 GVA Generator (man in foreground)

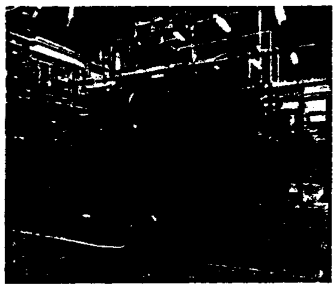

Seven 84 MVA Pulse-Shaping Power Supplies

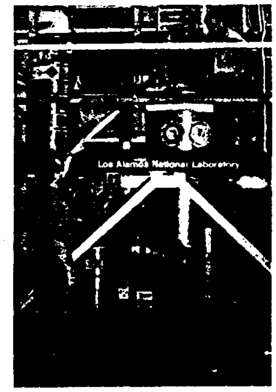

60T Long-Pulse Magnet

(38)

NHMFL Pulsed Magnet Facility in Los Alamos

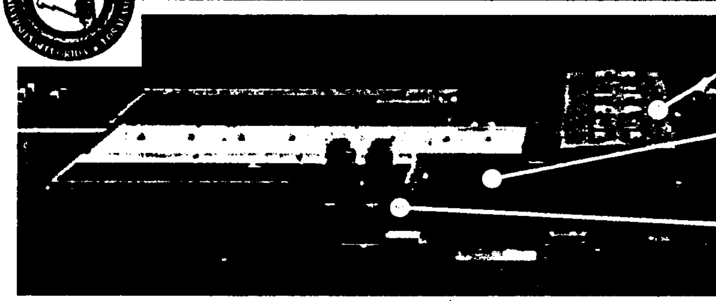

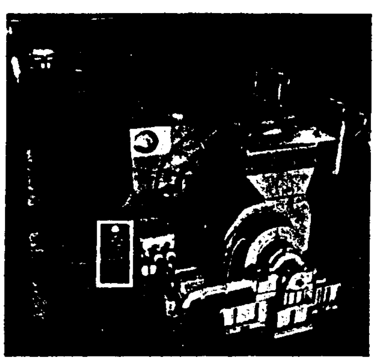

1.4 GVA Generator (man in foreground)

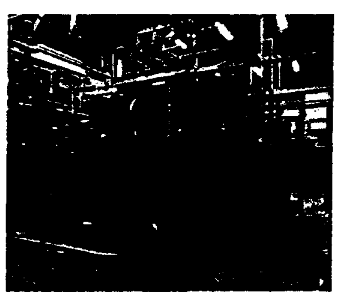

Seven 84 MVA Pulse-Shaping Power Supplies

Energy is stored in the power supply transformers.

Transistors update the voltage applied to the magnet roughly every msec.

The desired magnetic field pulse is shaped per the requirements of the experiment.

(41)

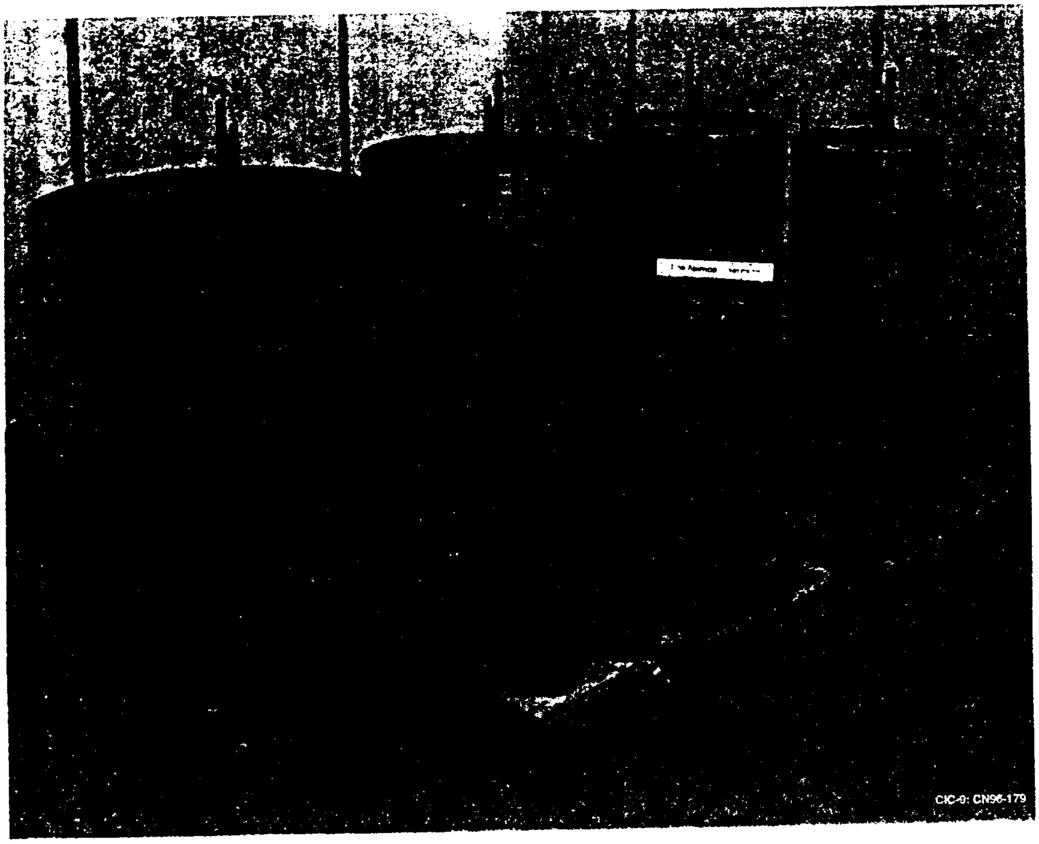

(40)

The 60T Long Pulse magnet.

Each pulse can be selected based upon the needs of the particular experiment.

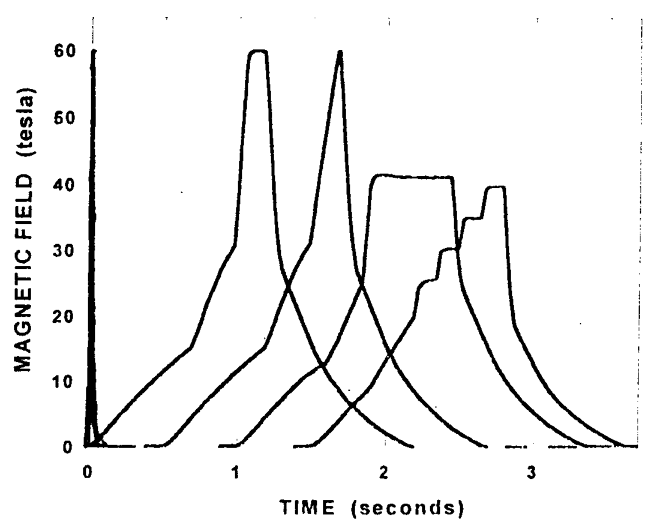

The magnetic length is 25 nanometers /$[B(\text{teslas})]^{1/2}$

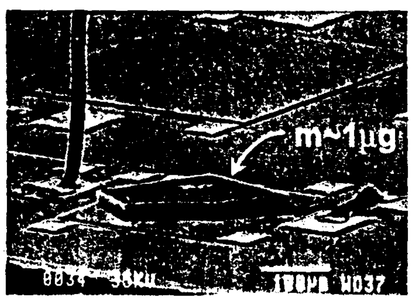

MEMS Magnetometer with SQUID sensitivity
Aksyuk, et al, Science 280 (1998) 720

Science in 60 Teslas
at the NHMFL
Pulsed Field Facility
in Los Alamos

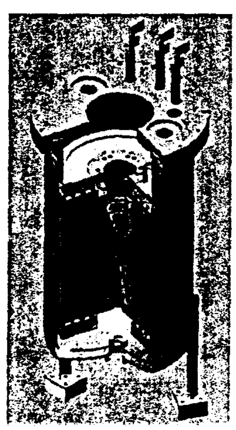

User Selectable
Pulse Shapes
Including
100msec at 60T

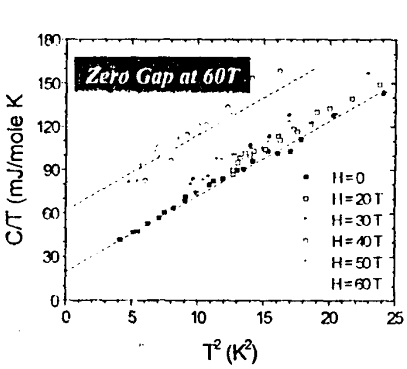

Specific Heat in a Kondo Insulator
Jaime, et al, Nature 405 (2000) 160

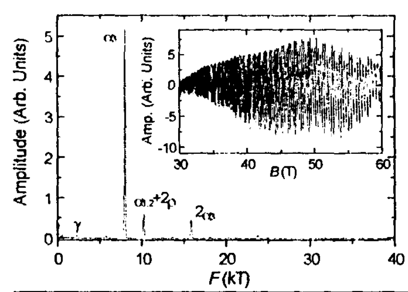

Magnetization in Heavy Fermion Alloys
Goodrich, et al, PRL 82 (1999) 3669

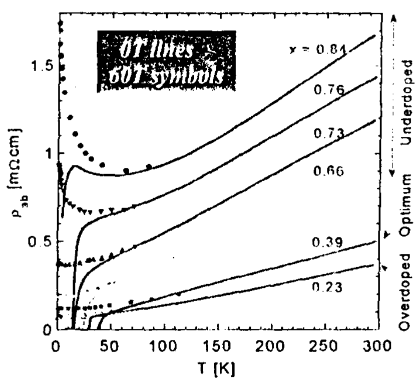

Transport in the High-Tc Superconductors
Ono, et al, PRL 85 (2000) 638
Morozov, et al, PRL 84 (2000) 1784